Supporting Information

In situ modification of d-band in core-shell structure for efficient hydrogen storage via electrocatalytic N_2 fixation

Xiaohui Yang [a,b#], Jin Wan[a#], Huijuan Zhang[a], Yu Wang [a,c*]

[a]School of Chemistry and Chemical Engineering, State Key Laboratory of Power Transmission Equipment & System Security and New Technology, Chongqing University, 174 Shazheng Street, Shapingba District, Chongqing City, 400044, P.R. China.

[b]Key Laboratory of Reservoir Aquatic Environment, Chongqing Institute of Green and Intelligent Technology, Chinese Academy of Sciences, No. 266, Fangzheng Avenue, Beibei District, Chongqing 400714, P.R. China.

[c]School of Electrical Engineering, Chongqing University, 174 Shazheng Street, Shapingba District, Chongqing City, 400044, P.R. China.

[#]These authors contributed equally to this work.

*Corresponding author. E-mail: wangy@cqu.edu.cn (Yu Wang)

Experimental Section

Chemicals and materials

All chemicals were used without any purification in this work. Vanadium pentoxide (V_2O_5, AR), sodium sulfate (Na_2SO_4, AR), zinc nitrate hexahydrate ($Zn(NO_3)_2·6H_2O$, AR), hexamethylenetetramine ($C_6H_{12}N_4$, AR), ammonium chloride (NH_4Cl, AR), hydrazine hydrate ($N_2H_4·H_2O$, AR), hydrochloric acid (HCl, AR), sulfuric acid (H_2SO_4), trisodium citrate dihydrate ($C_6H_5Na_3O_7·2H_2O$, AR), salicylic acid ($C_7H_6O_3$, AR), sodium hydroxide (NaOH, AR), sodium hypochlorite solution (NaClO) and ethanol were purchased from Chengdu Kelong Chemical Ltd. P-dimethylaminobenzaldehyde ($C_9H_{11}NO$, AR) and sodium pentacyanonitrosylferrate dihydrate ($Na_2Fe(CN)_5NO·2H_2O$, AR) was supplied by Aladdin Reagents Ltd. The water used throughout all experiments was purified through a Millipore system.

Synthesis of the precursor of $Zn_3(OH)_2(V_2O_7)(H_2O)_2$ nanosheets

A simple hydrothermal process was employed to synthesize the precursor based on the previous reports with appropriate modification. In a typical procedure, 1.5 mmol of V_2O_5, 3.5 mmol of Na_2SO_4, 1.0 mmol of $Zn(NO_3)_2·6H_2O$ and 2.5 mmol of $C_6H_{12}N_4$ were, in turn, dissolved in 30 ml distilled water, and then stirred vigorously until it becomes clear. Subsequently, this clear mixed solution was transferred into a 50 ml Teflon-lined stainless-steel autoclave, and then hydrothermally treated at 120 ℃ for 24 h. Finally, the nanosheet precursor was obtained from solution by centrifugation, washed with deionized water/ethanol, and then collected and dried at 60℃ in a vacuum.

Synthesis of 2D porous V_2O_3 nanomeshs

The 2D porous V_2O_3 nanomeshs were prepared by annealing the nanosheet precursor at 850℃ for 300 min under a mixture of 40%/60% Ar/H_2 flow.

Synthesis of controlled 2D core/shell V_2O_3/VN-X nanomeshs

The target samples of 2D core/shell V_2O_3/VN-X nanomeshs with gradient thickness of nitride shell were obtained via an accurate nitriding treatment, where the reaction conditions are under a mixture flow of Ar/NH_3 of 80%/20% at 700 ℃ and the thickness of nitride shell is controlled by regulating the nitriding time. Based on this, V_2O_3/VN-0.5, V_2O_3/VN-2, and V_2O_3/VN-10 were prepared, in which 0.5, 2, and 10 represent the reaction time of 0.5 min, 2 min, and 10 min, respectively. Furthermore, the pure VN nanomeshs were also prepared by extending the nitriding time to 200 min.

Characterization

The crystal structure of the as-synthesized samples was obtained by X-ray diffraction (XRD) on a Bruker D8 Advance diffractometer with Cu Ka radiation (λ=0.154 nm). The morphology and structure characterization were captured by field emission scanning electron microscopy (FESEM, JEOL JSM-7800F, 15kV), transmission electron microscopy (TEM, FEI, Talos F200S, 200kV） coupled with EDS analysis, and HAADF-STEM (FEI Titan Cubed Themis G2 300, 200 kV). X-ray photoelectron spectrometer (XPS) was employed to analyze the composition and valence states of samples on a Thermo Scientific ESCALAB 250Xi X-ray photoelectron spectrometer with a monochromatic Al Kα radiation (225W, 15mA, 15kV). UV-Vis spectra were conducted on a Shimadzu UV-3600 UV-Vis spectrophotometer. ^1H nuclear magnetic resonance (NMR) spectra were collected by a superconducting-magnet NMR spectrometer (Agilent, 600 DD2, 600 MHz).

Working Electrode Preparation

Primarily, 5 mg catalyst was dispersed in a mixed solution consisting of 50 μL Nafion (5 w%)

and 950 μL ethanol, and then a homogeneous ink was obtained by sonicating for 1 h. Subsequently, 80 μL of the ink was loaded onto a carbon paper with area of 1 cm × 1 cm and dried under ambient condition. Thus, the working electrode was obtained.

Electrochemical NRR Testing

The NRR tests were measured in a two-compartment electrolytic cell separated by a Nafion-1035 proton exchange membrane. Before the NRR tests, this Nafion membrane was pretreated by boiling in H_2O_2 (3%) aqueous solution at 120 ℃ for 0.5 h. Then, it was boiled in 0.5 M H_2SO_4 solution for 1 h and rinsed in ultrapure water several times. The electrochemical tests were conducted on a typical three-electrode system, where the as-synthesized working electrode and the reference electrode of Ag/AgCl were placed in cathode compartment, while the Pt foil as the counter electrode was placed in anode compartment. In this work, all potentials were converted to reversible hydrogen electrode (RHE) and calibration with the following equation: E (vs RHE) = E (vs Ag/AgCl) + 0.21 + 0.059 × pH (in 3 M aqueous KCl corresponding to the standard potential of Ag/AgCl, E°Ag/AgCl = 0.21 V), and the displayed current density was normalized to the geometric surface area. In the process of electrochemical NRR, high-purify N_2 was first injected into the 0.05 M H_2SO_4 solution (pH=1) for at least 30 min to remove the residual air in the cathode compartment. The potentiostatic tests were performed at -0.1 V, -0.2 V, -0.3 V, -0.4 V, -0.5 V and -0.6 V, respectively.

Determination of ammonia

The concentration of produced NH_3 was detected via an indophenol blue method. Primarily, 2 mL electrolyte was removed from the cathode compartment and mixed with the 2 mL NaOH solution consisting of 5 wt% salicylic acid and 5 wt% sodium citrate. Then, 1 mL of 0.05 M NaClO and 0.2 mL of 1 wt% sodium nitroferricyanide ($C_5FeN_6Na_2O$) were successively added into the above solution and standed for 2 h in the dark environment. Subsequently, the absorption spectrum was measured using an UV-Vis spectrophotometer at λ = 655 nm. Besides, the standard curve was achieved by measuring a series of absorbances for the reference solutions with different NH_4Cl concentrations (0, 0.2 μg mL^{-1}, 0.5 μg mL^{-1}, 1 μg mL^{-1}, 1.5 μg mL^{-1}, 2 μg mL^{-1}, 3 μg mL^{-1}) in 0.05 M H_2SO_4 solution (Figure S5).

Determination of Hydrazine

The amount of hydrazine in electrolyte was estimated by the method of Watt and Chrisp. Typically, a mixed solution consisting of 5.99 g $C_9H_{11}NO$, 30 ml of HCl, and 300 ml of ethanol was synthesized as the color reagent. Then, 5 mL of the electrolyte solution was collected and mixed with 5 mL of the color reagent. After stirring in the dark for 20 min, the absorption spectrum was measured at λ = 458 nm. Similarly, the standard curve was achieved by measuring a series of absorbances for the reference solutions with different N_2H_4 concentrations (0, 0.2 μg mL^{-1}, 0.4 μg mL^{-1}, 0.6 μg mL^{-1}, 0.8 μg mL^{-1}, 1.0 μg mL^{-1}, 2.0 μg mL^{-1}) in 0.05 M H_2SO_4 solution (Figure S6).

Calculation of the yield rate and the Faradaic efficiency

The NH_3 yield rate (v_{NH_3}) is obtained using the following equation:

$$v_{NH_3} = (c_{NH_3} \times V)/(t \times m_{cat.}) \quad (1)$$

The Faradaic efficiency (FE) is estimated by the ratio of the charge consumed for NH_3 generation to the quantity of total applied electricity (C), with an assumption that three electrons are consumed to produce one NH_3 molecule:

$$FE = (3 \times F \times c_{NH_3} \times V)/(17 \times Q) \quad (2)$$

where c_{NH_3} is the mass concentration of measured NH_3; V is the electrolyte volume; t is the reduction time (1h); $m_{cat.}$ is the loading mass of catalyst; F is the faraday constant (96 485 C mol^{-1}); Q is the

quantity of total applied electricity (C).

The normalized v_{NH_3} can be calculated by the equation:

$$\text{Normalized } v_{NH_3} = (c_{NH_3} \times V)/(t \times A \times \text{RF}) \quad (3)$$

where RF is the roughness factor.

Computational Methods

All the calculations were conducted by the spin-polarized density functional theory (DFT) with the projector-augmented-wave pseudopotential (PAW)[1] implemented in Vienna ab initio Simulation Package (VASP).[2-5] The Perdew-Burke-Ernzerhof (PBE) functional was performed to describe the exchange-correlation energy.[6] Considering the strong correlation among the electrons of transition metal oxides, the GGA + U approach was adopted.[7] The effective U value for V was set to 2.5.[8] A cutoff energy of 500 eV for the plane-wave basis was adopted. The energy convergence criteria was set to 10^{-5} eV. The force convergence in self-consistent field was 0.03 eV/Å for the geometry optimization. A vacuum space of 10 Å along the z-direction was used to prevent interactions between periodic images. The Brillouin zone was sampled using a 2 × 2 × 1 grid centered at the gamma (Γ) point for fully relaxed geometry optimization, while a 4 × 4 × 1 k-points grid was employed for electronic property computations.

The Gibbs free energy (G) of each NRR intermediates was calculated based on the computational hydrogen electrode (CHE) model proposed by Nørskov et al[9]. The chemical potential of proton/electron (H^+/e^-) pair in aqueous solution is equal to half of the H_2 gas molecule at standard hydrogen electrode (SHE) conditions. According to CHE model, the G can be defined as follows:

$$G = \Delta E - T\Delta S + \Delta E_{ZPE} + \Delta G_U + \Delta G_{pH} \quad (4)$$

Where ΔE is the total energy directly obtained by DFT calculations, and T is the temperature (T=298.15 K). ΔE_{ZPE} and ΔS are the differences of zero-point energy and entropy, respectively. ΔG_U is the free energy contribution related to applied potential U, which can be determined as $\Delta G_U = -eU$. The U value is determined by the equation $U = -\Delta G_{max}/e$, where ΔG_{max} is free energy change in potential-determining step. ΔG_{pH} is the correction of the free energy of H^+ ions by the concentration dependence of the entropy: $\Delta G_{pH} = 2.303 \times kB \times pH$, where kB is the Boltzmann constant, and the value of pH is set to be 0 at acid conditions.

where ΔE is the reaction energy difference, ΔE_{ZPE} and ΔS are the difference in the zero-point energy and entropy obtained. In addition, the adsorption energy (E_{ad}) of adsorbate is defined as:

$$E_{ad} = E_{M*} - E_* - E_M \quad (5)$$

where E_{M*}, E_*, and E_M, are total energies of catalyst with adsorbates, the isolate catalyst, and the corresponding adsorbates, respectively.

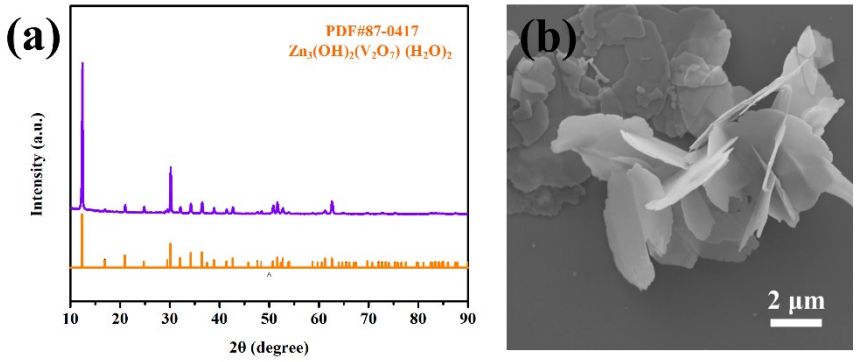

Figure S1. (a) XRD pattern and (b) SEM image of the precursor for $Zn_3(OH)_2(V_2O_7)(H_2O)_2$ nanosheets.

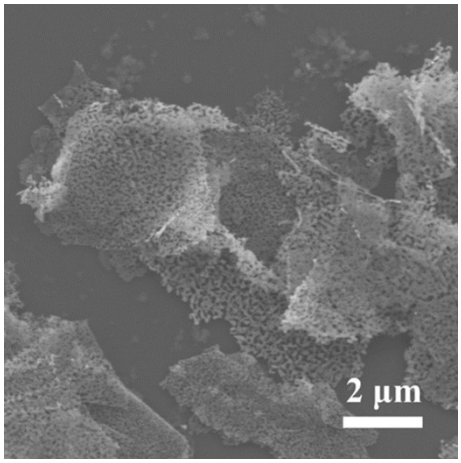

Figure S2. SEM image of the core V_2O_3 nanomeshs

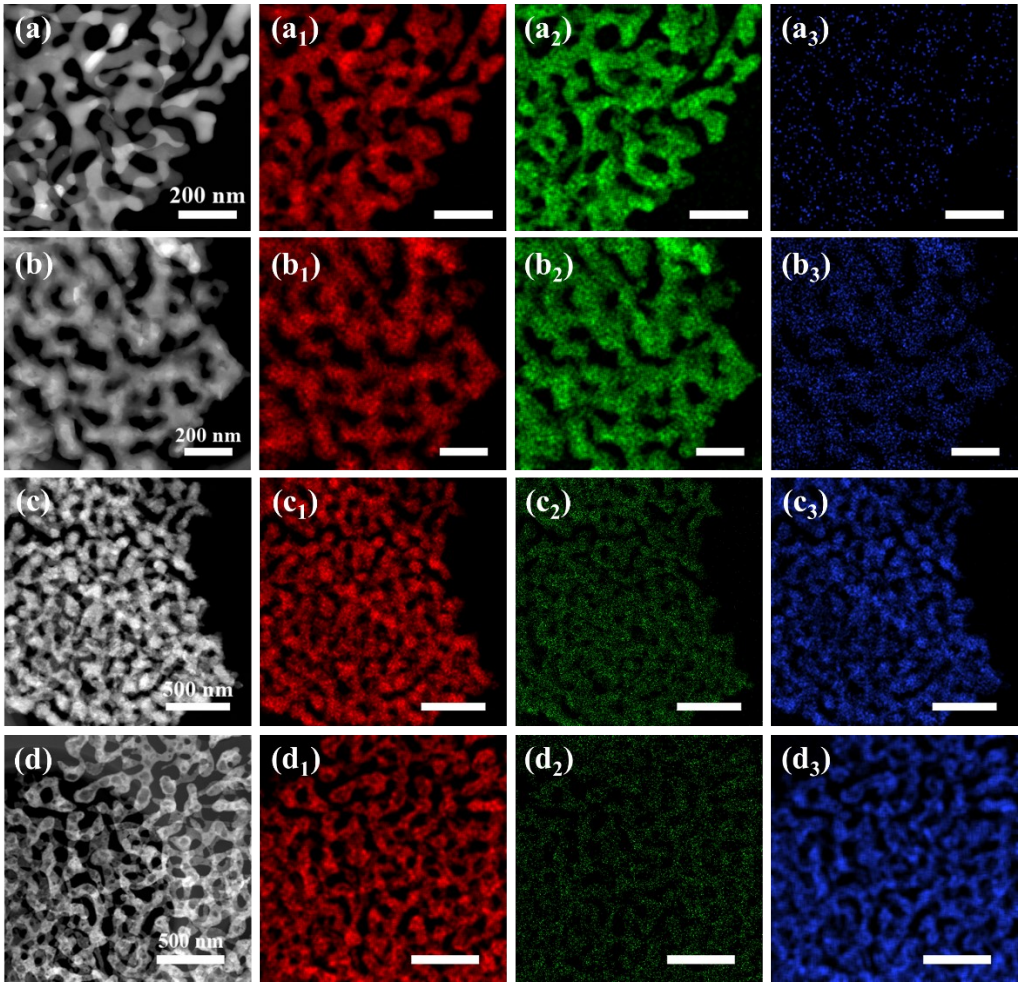

Figure S3. HAADF-STEM images of (a) 2D porous V_2O_3/VN-0.5, (b) 2D porous V_2O_3/VN-2, (c) 2D porous V_2O_3/VN-10, (d) 2D porous pure VN. The corresponding EDS elemental mapping images of (a_1-d_1) V, (a_2-d_2) O, and (a_3-d_3) N based on image **a**, **b**, **c**, **d**, respectively.

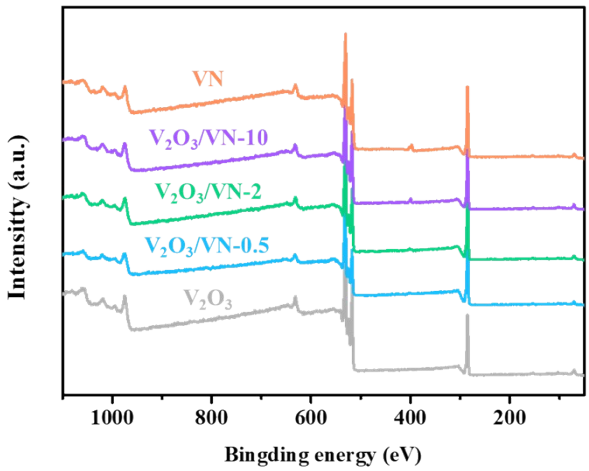

Figure S4. XPS full spectra of pure V_2O_3, V_2O_3/VN-0.5, V_2O_3/VN-2, V_2O_3/VN-10, and pure VN.

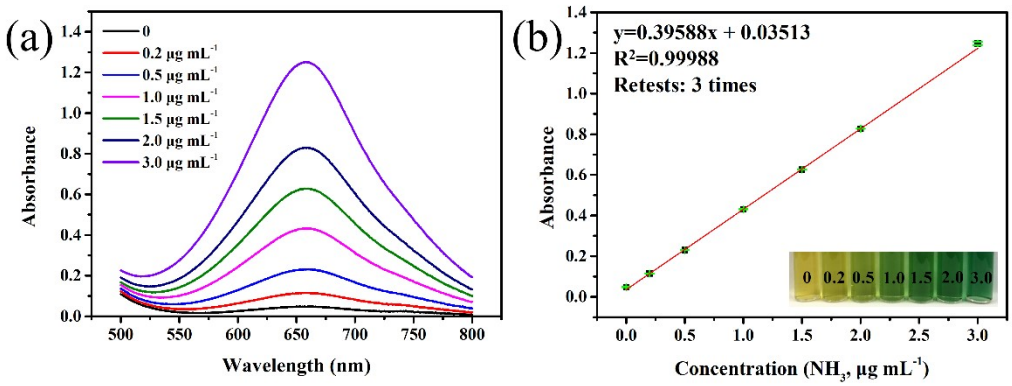

Figure S5. (a) UV-vis curves of indophenol assays with NH_4^+ ions (ammonium chloride solutions of known concentration) after being incubated for 2 h at room temperature. (b) calibration curve used for estimation of NH_3 by NH_4^+ ion concentration. The absorbance at 655 nm was measured by UV-vis spectrophotometer. The standard curve showed good linear relation of absorbance with NH_4^+ ion concentration ($y = 0.39588x + 0.03513$, $R^2 = 0.99988$) of three times independent calibration curves. The inset in **b** shows the chromogenic reaction of indophenol indicator with NH_4^+ ions.

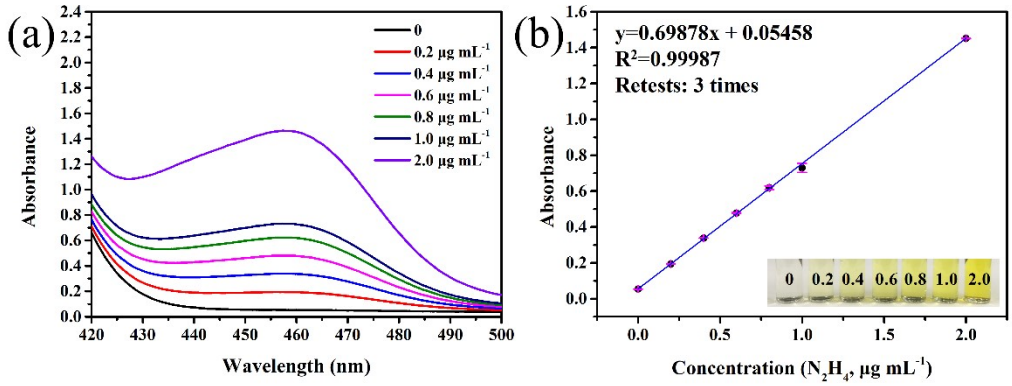

Figure S6. (a) UV-Vis absorption spectra of various N_2H_4 concentration after incubated for 20 min at room temperature. (b) Calibration curve used for calculation of N_2H_4 concentration. The absorbance at 458 nm was measured by UV-vis spectrophotometer. The inset in **b** shows the chromogenic reaction of para-dimethylamino-benzaldehyde indicator with N_2H_4.

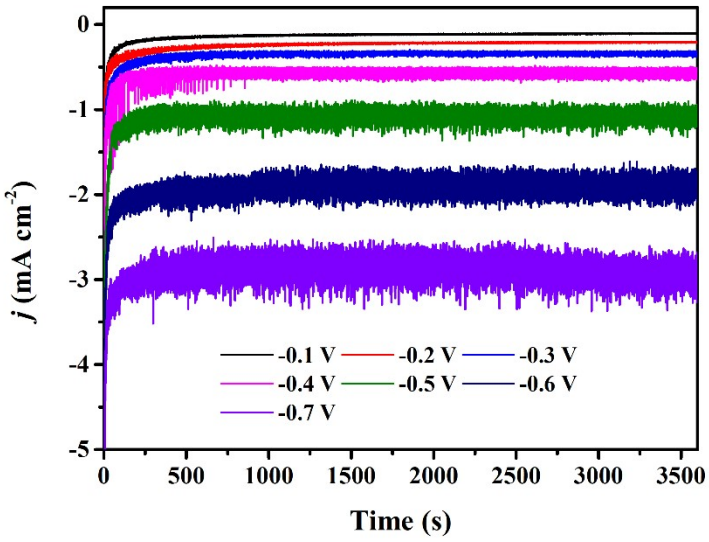

Figure S7. Chronoamperometry curves of 2D Core/Shell V_2O_3/VN nanomeshs at different applied potentials in N_2-saturated 0.05 M H_2SO_4 solution.

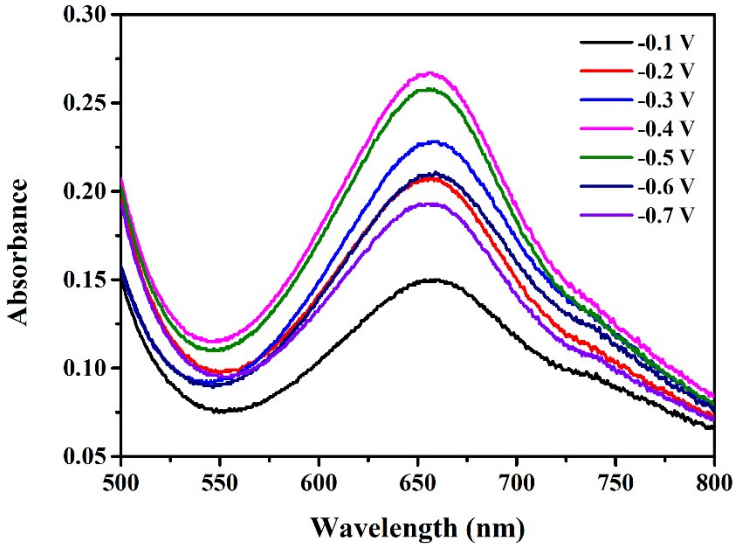

Figure S8. UV-Vis absorption spectra of the electrolytes colored with indophenol indicator after 1 h electrolysis in N_2 at various potentials under ambient conditions.

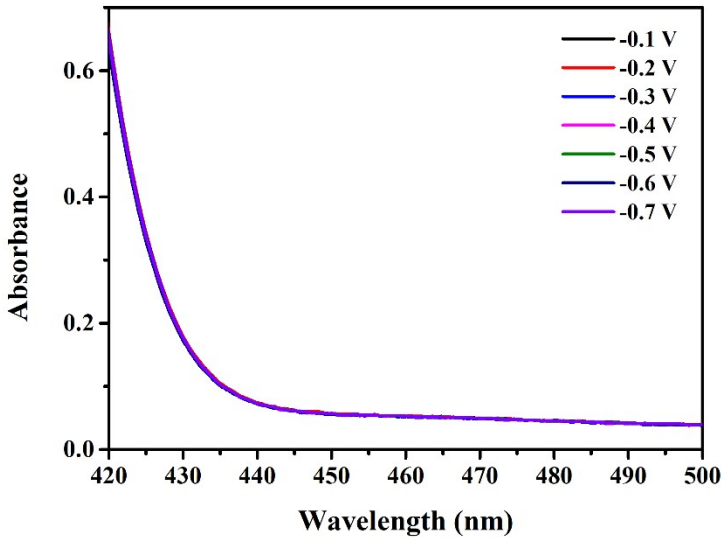

Figure S9. UV-Vis absorption spectra of the electrolytes stained with para-dimethylamino-benzaldehyde indicator after 1 h electrolysis in N_2 at various potentials under ambient conditions.

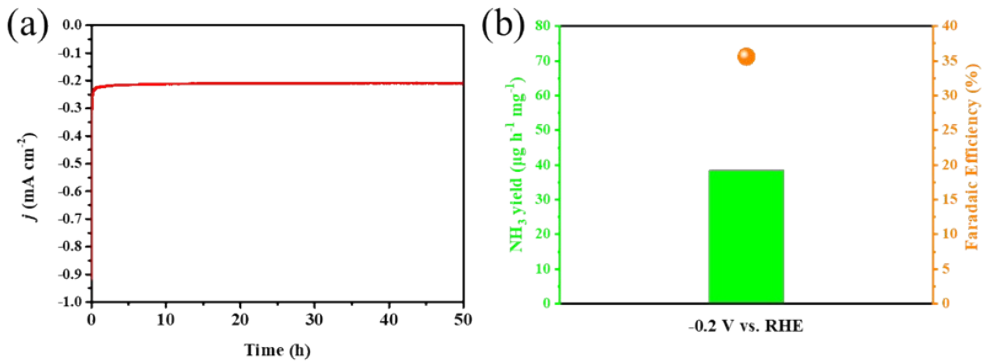

Figure S10. (a) Time-dependent current density curve of 2D Core/Shell V_2O_3/VN-2 nanomeshs in N_2-saturated 0.05 M H_2SO_4 solution at -0.2 V vs. RHE. (b) The NH_3 yield and FE at -0.2 vs. RHE after long-term electrocatalytic test of 50 h.

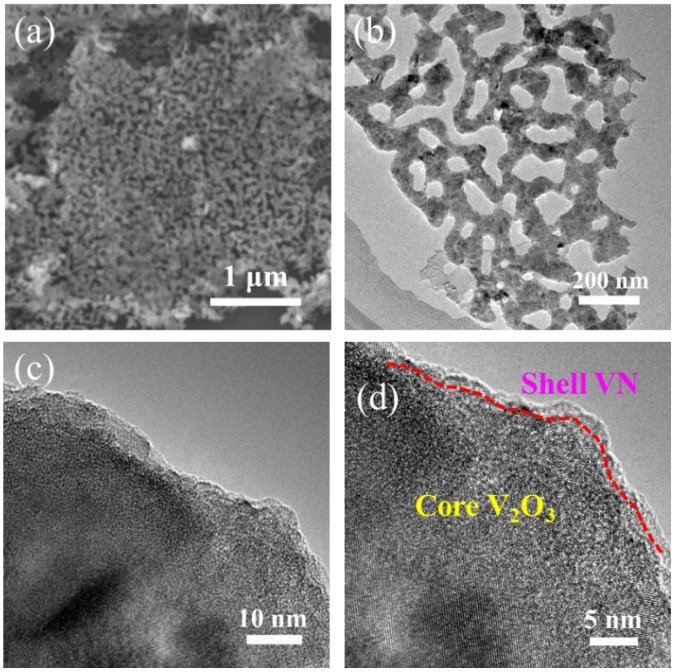

Figure S11. (a) SEM image, (b) TEM image, (c) and (d) High-resolution TEM images for 2D Core/Shell V_2O_3/VN-2 nanomeshs after the electrocatalysis.

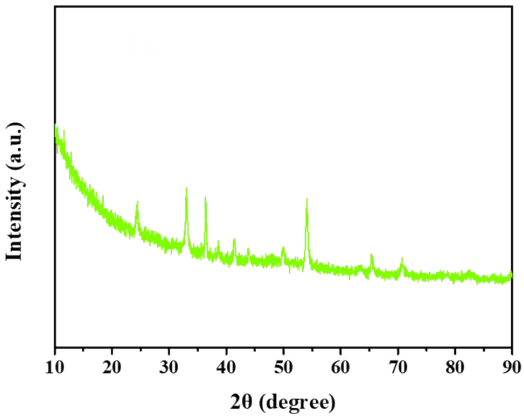

Figure S12. XRD pattern of 2D Core/Shell V_2O_3/VN-2 nanomeshs after electrocatalysis.

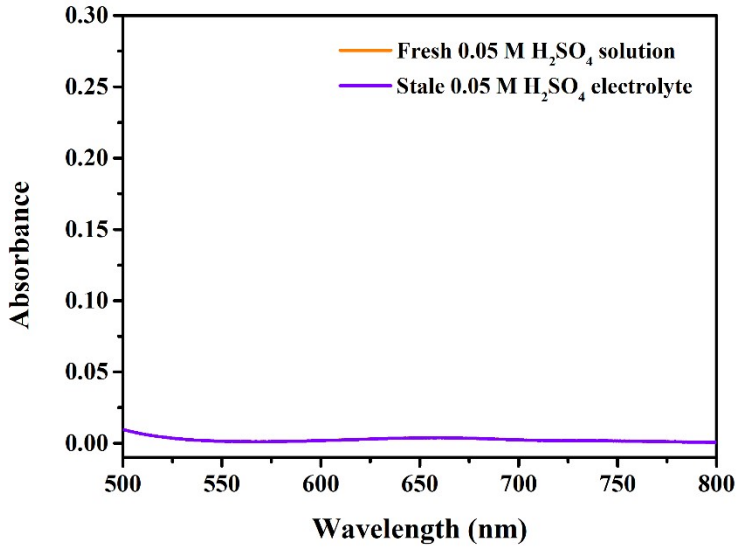

Figure S13. UV-Vis absorption spectra of blank experiments with the fresh 0.05 M H_2SO_4 solution and the stale 0.05 M H_2SO_4 electrolyte treated by N_2 gas bubbling for 1h, which are colored with indophenol indicator.

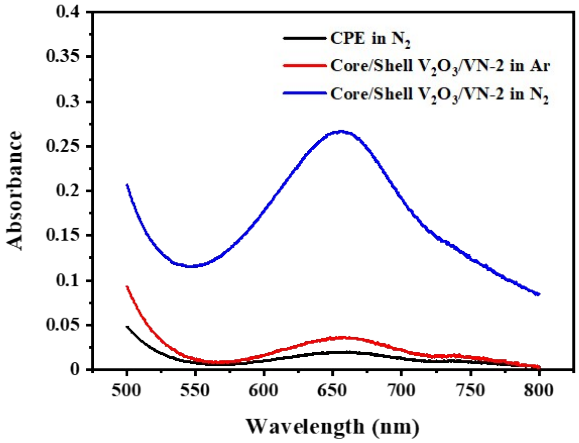

Figure S14. UV-vis absorption spectra of the electrolytes stained with indophenol indicator after charging at -0.4 V vs. RHE for 1 h under various conditions

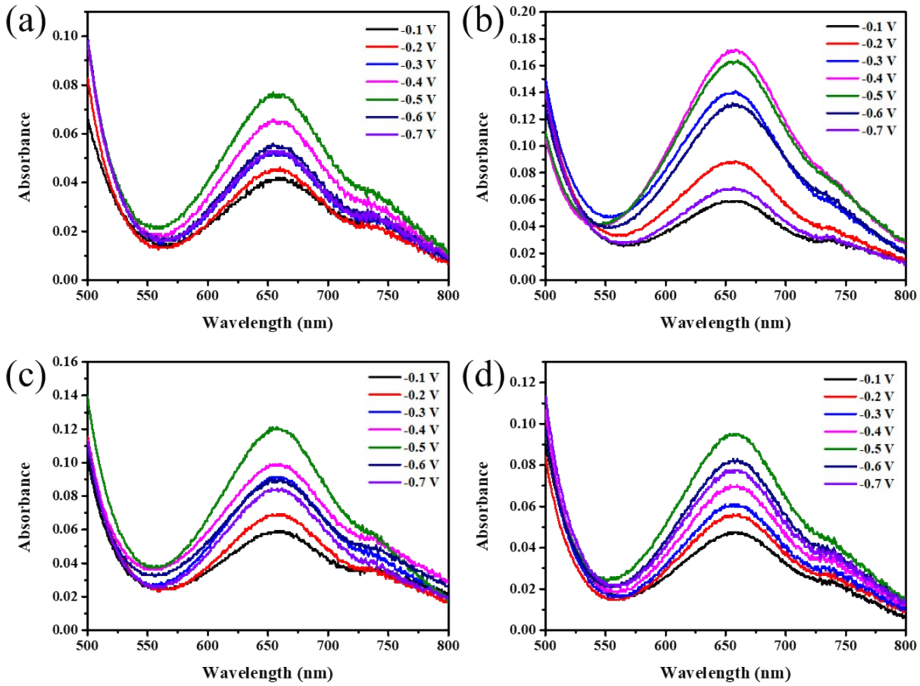

Figure S15. UV-Vis absorption spectra of the electrolytes stained with indophenol indicator at different applied potentials over (a) pure V_2O_3 nanomeshs, (b) core/shell V_2O_3/VN-0.5 nanomeshs, (c) core/shell V_2O_3/VN-10 nanomeshs, and (d) pure VN nanomeshs

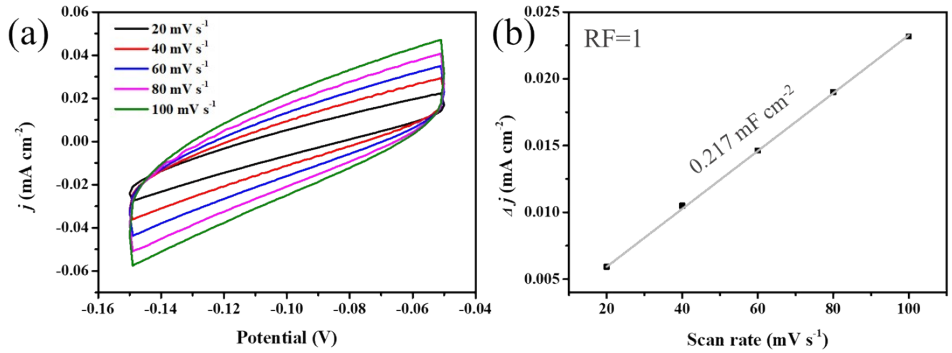

Figure S16. (a) Cyclic voltammetry curves of pure V_2O_3 nanomeshs at various rates (20, 40, 60, 80, and 100 mV s^{-1}), respectively. (b) The corresponding plots of the current density variation at -0.1 V vs. the scan rate. Here, we suppose that roughness factor (RF) value of pure V_2O_3 nanomeshs sample is 1.

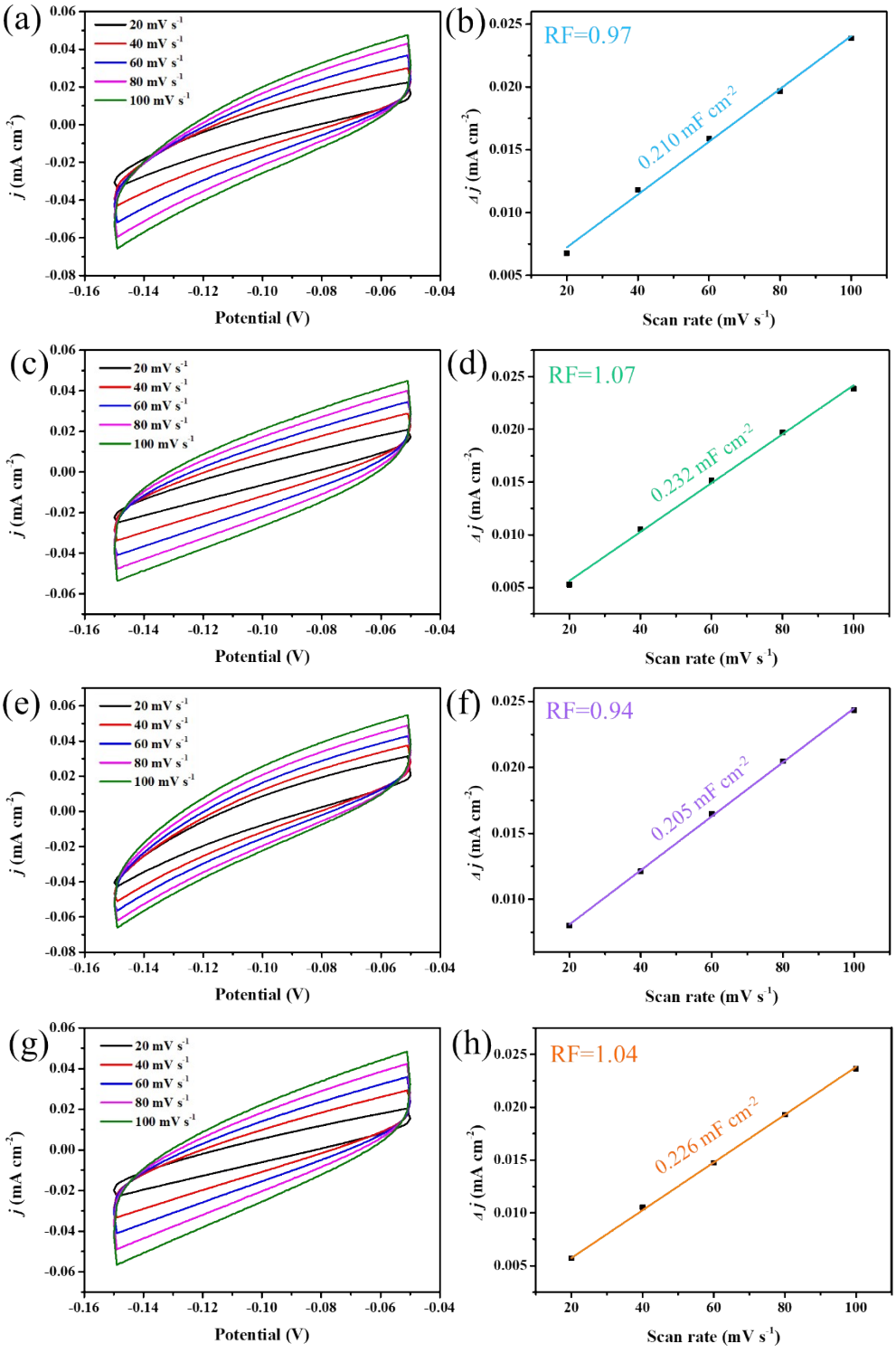

Figure S17. Cyclic voltammetry curves of core/shell V_2O_3/VN-0.5 nanomeshs (a), core/shell V_2O_3/VN-2 nanomeshs (c) core/shell V_2O_3/VN-10 nanomeshs (e) and pure VN nanomeshs (g). at various rates (20, 40, 60, 80, and 100 mV s^{-1}), respectively. (b), (d), (f), and (h) The corresponding plots of the current density variation at -0.1 V vs. the scan rate. RFs in insets were calculated by dividing the capacitances of core/shell V_2O_3/VN-X and pure VN nanomeshs by the C_{dl} value of pure V_2O_3 nanomeshs with an assumption that its RF value is 1.

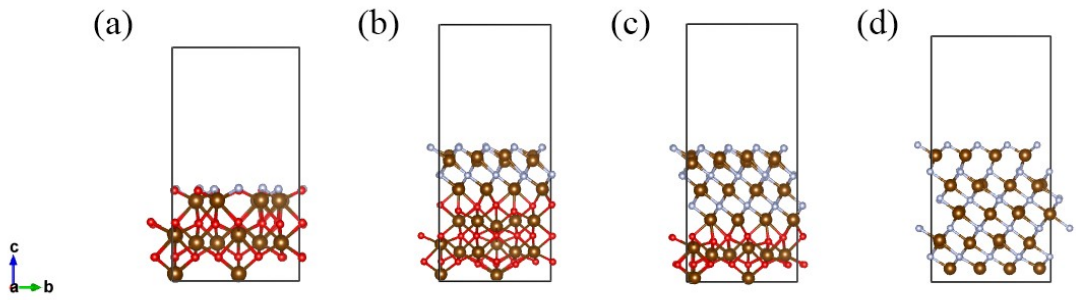

Figure S18. Structural prototype of these four systems. (a) V_2O_3/N-doped, (b) V_2O_3/VN-2 layer, (c) V_2O_3/VN-3 layer, (d) pure VN. The brown, red, and gray balls represent the V, O, and N atoms, respectively.

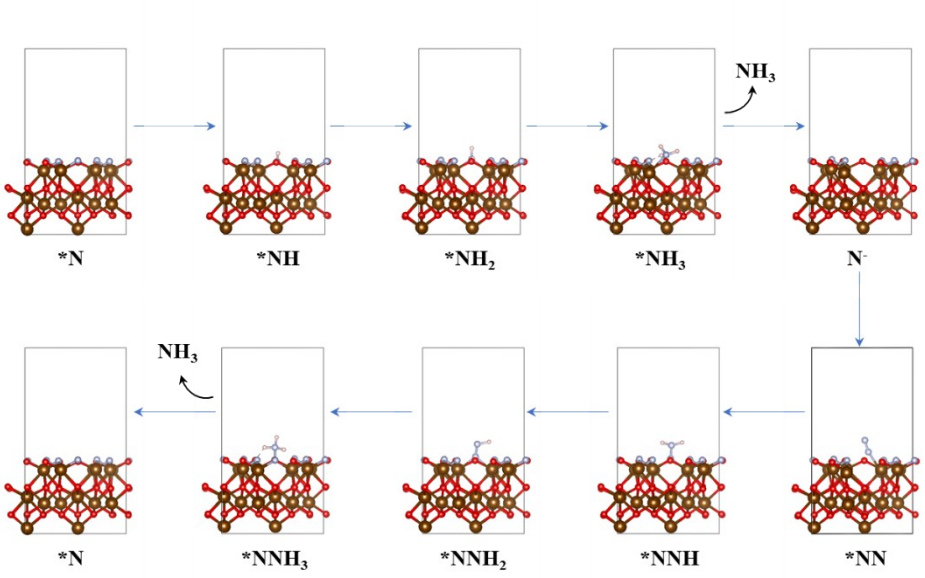

Figure S19. Atomistic structure schemes showing the MvK pathway of the N_2 reduction over V_2O_3/N-doped.

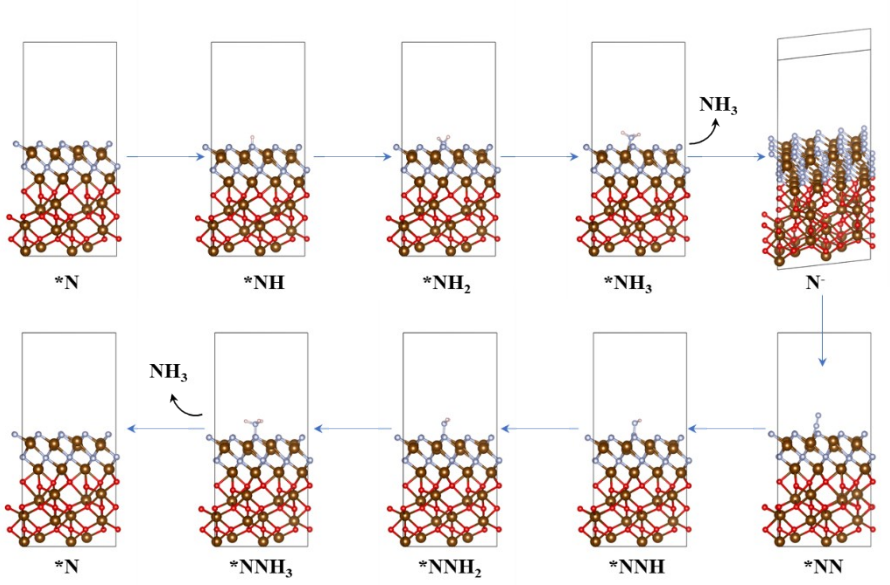

Figure S20. Atomistic structure schemes showing the MvK pathway of the N_2 reduction over V_2O_3/VN-2 layer.

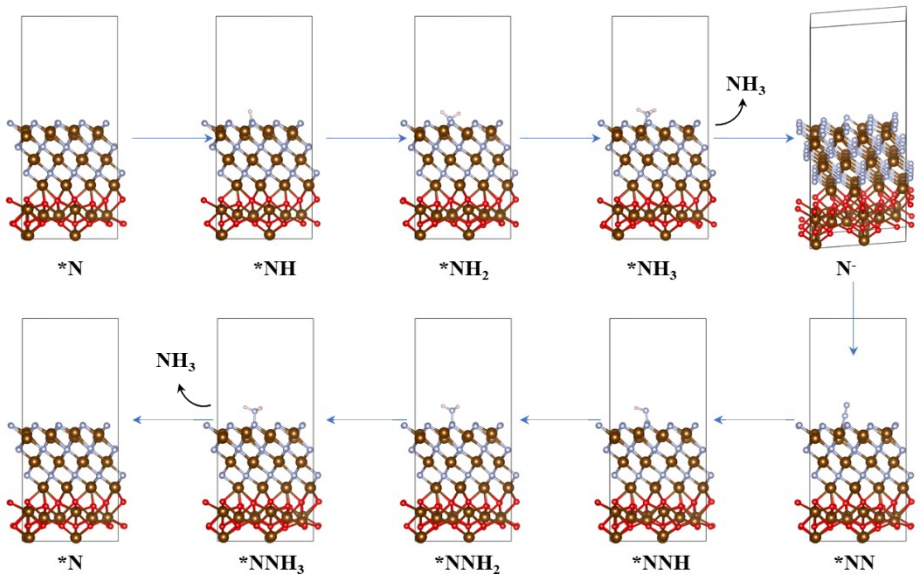

Figure S21. Atomistic structure schemes showing the MvK pathway of the N_2 reduction over V_2O_3/VN-3 layer.

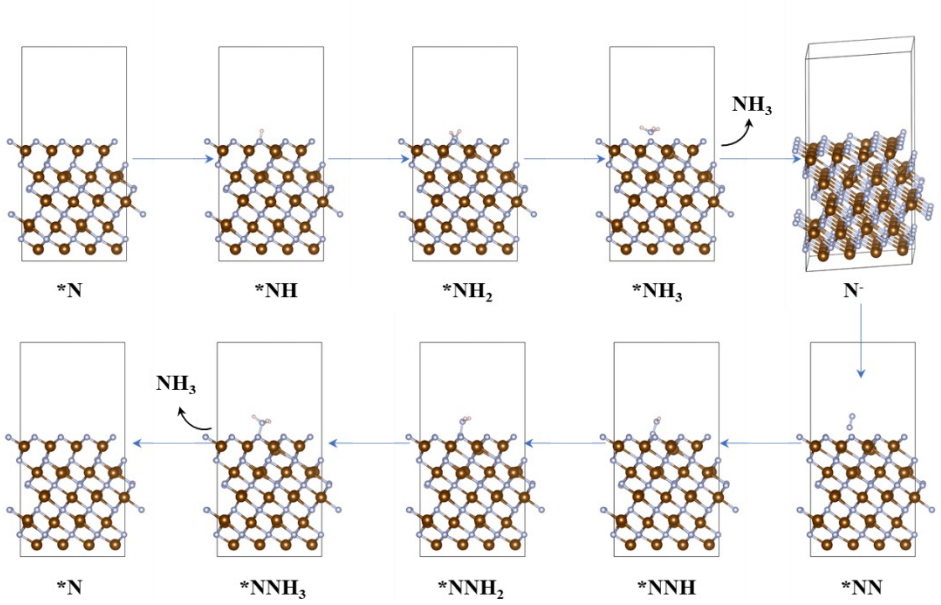

Figure S22. Atomistic structure schemes showing the MvK pathway of the N_2 reduction over pure VN.

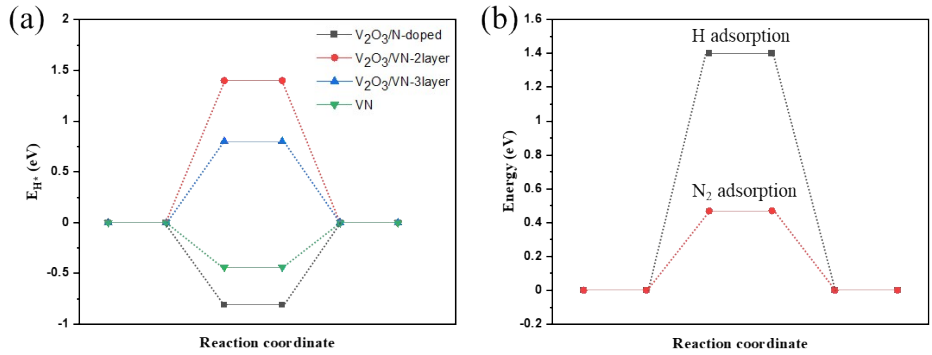

Figure S23. (a) H adsorption energy comparisons for V_2O_3/N-doped, V_2O_3/VN-2 layer, V_2O_3/VN-3 layer, and pure VN. (b) Adsorption energy comparisons of N_2 and H over V_2O_3/VN-2 layer.

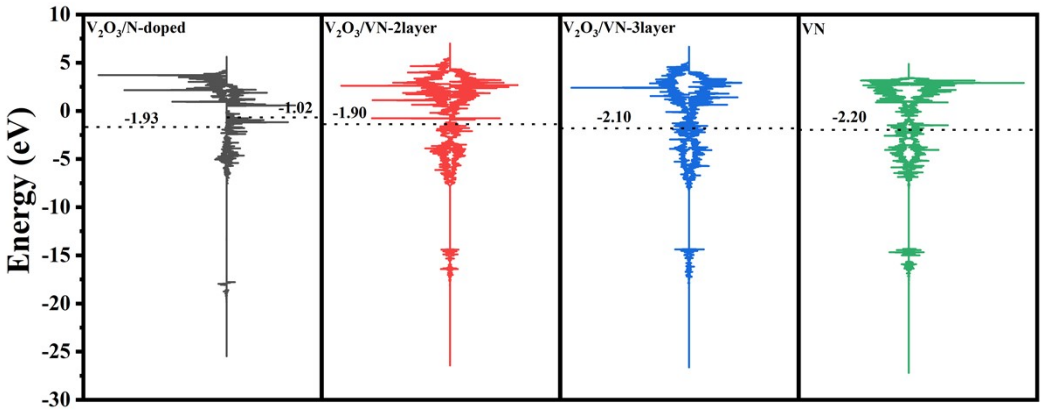

Figure S24. The d-band state of these four systems. The dash line highlight the d-band center.

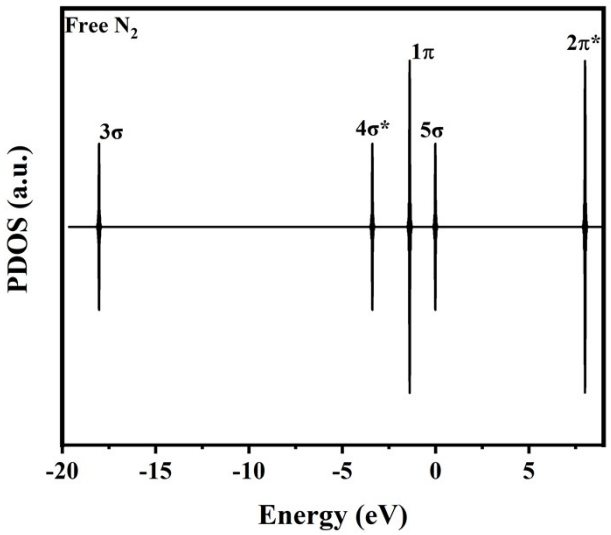

Figure S25. The molecular orbitals of free N_2.

Table S1. Comparison of electrochemical N_2 reduction performance for 2D core/shell V_2O_3/VN nanomeshs with recently reported advanced electrocatalysts in acid electrolyte under ambient conditions.

Catalyst	Electrolyte	Temperature	NH_3 Yield Rate	FE	Reference
2D core/shell V_2O_3/VN nanomeshs	**0.05 M H_2SO_4**	**Room temperature**	**59.7 μg h^{-1} $mg^{-1}_{cat.}$**	**34.9%**	**This work**
SA-Mo/NPC	0.1 M HCl	Room temperature	31.5 μg h^{-1} $mg^{-1}_{cat.}$	6.7%	[10]
B_4C	0.1 M HCl	Room temperature	26.57 μg h^{-1} $mg^{-1}_{cat.}$	15.95%	[11]
Boron-doped graphene	0.05 M H_2SO_4	25 °C	9.8 μg h^{-1} cm^{-2}	10.8%	[12]
N-doped porous carbon	0.05 M H_2SO_4	Room temperature	1.40 mmol g^{-1} h^{-1}	1.42%	[13]
OVs-MoO_2	0.1 M HCl	Room temperature	12.20 μg h^{-1} $mg^{-1}_{cat.}$	10.04%	[14]
Oxygen-Vacancy-Rich $TiO_2/Ti_3C_2T_x$	0.1 M HCl	Room temperature	32.17 μg h^{-1} $mg^{-1}_{cat.}$	16.07%	[15]
Amorphous $Bi_4V_2O_{11}/CeO_2$	0.1 M HCl	Room temperature	23.21μg h^{-1} $mg^{-1}_{cat.}$	10.16%	[16]
PCN-NV4	0.1 M HCl	Room temperature	8.09 μg h^{-1} $mg^{-1}_{cat.}$	11.59%	[17]
Bi nanodendrites	0.1 M HCl	Room temperature	25.86 μg h^{-1} $mg^{-1}_{cat.}$	10.8%	[18]
BiNi alloy	0.1 M Na_2SO_4	Room temperature	17.5 μg h^{-1} $mg^{-1}_{cat.}$	13.8%	[19]

2D c-COFs with Fe–N_4–C	0.01 M H_2SO_4	Room temperature	33.6 μg h^{-1} $mg^{-1}_{cat.}$	31.9%	[20]
CoS_2/NS-G	0.05 M H_2SO_4	Room temperature	25.0 μg h^{-1} $mg^{-1}_{cat.}$	25.9%	[21]

References

1. P. E. Blochl, *Phys. Rev. B*, 1994, **50**, 17953-17979.
2. G. Kresse and J. Furthmuller, *Comp. Mater. Sci.*, 1996, **6**, 15-50.
3. G. Kresse and J. Furthmuller, *Phys. Rev. B*, 1996, **54**, 11169-11186.
4. G. Kresse and D. Joubert, *Phys. Rev. B*, 1999, **59**, 1758-1775.
5. S. Grimme, J. Antony, S. Ehrlich and H. Krieg, *J. Chem. Phys.*, 2010, **132**, 154104.
6. J. P. Perdew, K. Burke and M. Ernzerhof, *Phys. Rev. Lett.*, 1996, **77**, 3865-3868.
7. F. A. a. A. I. L. Vladimir I Anisimov†, *J. Phys-Condens. Mat.*, 1997, **9**, 767–808.
8. J. Zhang, R.-J. Zhou, Q.-Y. Chang, Z.-J. Sui, X.-G. Zhou, D. Chen and Y.-A. Zhu, *Catal Today*, 2021, **368**, 46-57.
9. J. K. Nørskov, J. Rossmeisl, A. Logadottir, L. Lindqvist, J. R. Kitchin, T. Bligaard and H. Jonsson, *J. Phys. Chem. B*, 2004, **108**, 17886-17892.
10. L. Han, X. Liu, J. Chen, R. Lin, H. Liu, F. Lue, S. Bak, Z. Liang, S. Zhao, E. Stavitski, J. Luo, R. R. Adzic and H. L. Xin, *Angew. Chem. Int. Ed.*, 2019, **58**, 2321-2325.
11. W. Qiu, X. Y. Xie, J. Qiu, W. H. Fang, R. Liang, X. Ren, X. Ji, G. Cui, A. M. Asiri, G. Cui, B. Tang and X. Sun, *Nat. Commun.*, 2018, **9**, 3485.
12. X. Yu, P. Han, Z. Wei, L. Huang, Z. Gu, S. Peng, J. Ma and G. Zheng, *Joule*, 2018, **2**, 1610-1622.
13. Y. Liu, Y. Su, X. Quan, X. Fan, S. Chen, H. Yu, H. Zhao, Y. Zhang and J. Zhao, *ACS Catal.*, 2018, **8**, 1186-1191.
14. W. Cheng, X. Zhao, H. Su, F. Tang, W. Che, H. Zhang and Q. Liu, *Nat. Energy*, 2019, **4**, 115-122.
15. Y. Fang, Z. Liu, J. Han, Z. Jin, Y. Han, F. Wang, Y. Niu, Y. Wu and Y. Xu, *Adv. Energy Mater.*, 2019, **9**, 1803406.
16. C. Lv, C. Yan, G. Chen, Y. Ding, J. Sun, Y. Zhou and G. Yu, *Angew. Chem. Int. Ed.*, 2018, **57**, 6073-6076.
17. C. Lv, Y. Qian, C. Yan, Y. Ding, Y. Liu, G. Chen and G. Yu, *Angew. Chem. Int. Ed.*, 2018, **57**, 10246-10250.
18. F. Wang, X. Lv, X. Zhu, J. Du, S. Lu, A. A. Alshehri, K. A. Alzahrani, B. Zheng and X. Sun, *Chem. Commun.*, 2020, **56**, 2107-2110.
19. Z. Fang, P. Wu, Y. Qian and G. Yu, *Angew. Chem. Int. Ed.*, 2021, **60**, 4275-4281.
20. H. Zhong, M. Wang, M. Ghorbani-Asl, J. Zhang, K. H. Ly, Z. Liao, G. Chen, Y. Wei, B. P. Biswal, E. Zschech, I. M. Weidinger, A. V. Krasheninnikov, R. Dong and X. Feng, *J. Am. Chem. Soc.*, 2021, **143**, 19992-20000.
21. P. Chen, N. Zhang, S. Wang, T. Zhou, Y. Tong, C. Ao, W. Yan, L. Zhang, W. Chu, C. Wu and Y. Xie, *Proc. Natl Acad. Sci.*, 2019, **116**, 6635-6640.